

Strong gravitational lensing by a rotating non-Kerr compact object

Songbai Chen^{*}, Jiliang Jing[†]

*Institute of Physics and Department of Physics, Hunan Normal University,
Changsha, Hunan 410081, People's Republic of China
Key Laboratory of Low Dimensional Quantum Structures
and Quantum Control of Ministry of Education, Hunan Normal University,
Changsha, Hunan 410081, People's Republic of China*

Abstract

We study the strong gravitational lensing in the background of a rotating non-Kerr compact object with a deformed parameter ϵ and an unbound rotation parameter a . We find that the marginally circular stable orbit radius and the deflection angle depend sharply on the parameters ϵ and a . For the case in which the black hole is more prolate than a Kerr black hole, the marginally circular photon orbit exists only in the regime $\epsilon \leq \epsilon_{max}$ for a prograde photon. The upper limit ϵ_{max} is a function of the rotation parameter a . As $\epsilon > \epsilon_{max}$, the deflection angle of the light ray very close to the naked singularity is a positive finite value, which is different from that in the rotating naked singularity described by Janis-Newman-Winicour metric. For the oblate black hole and the retrograde photon, there does not exist such a threshold value. Modeling the supermassive central object of the Galaxy as a rotating non-Kerr compact object, we estimated the numerical values of the coefficients and observables for gravitational lensing in the strong field limit.

PACS numbers: 04.70.Dy, 95.30.Sf, 97.60.Lf

^{*} csb3752@hunnu.edu.cn

[†] jljing@hunnu.edu.cn

I. INTRODUCTION

The no-hair theorem [1] tells us that a neutral rotating black hole in asymptotically flat and matter-free spacetime is described completely by the Kerr metric with only two parameters, the mass M and the rotation parameter a , which means that all astrophysical black holes in our Universe should be Kerr black holes. Since the current observational data show that there is still lacking a definite proof for the existence of black holes in our Universe, several potential methods have been proposed to test the no-hair theorem by making use of observations including gravitational waves from extreme mass-ratio inspirals [2–5] and the electromagnetic spectrum emitted by the accreting disk around black holes [6, 7], and so on. These techniques are based on spacetimes which deviate from the Kerr metric by one or more parameters [4, 5, 8, 9]. Only if all these deviations are measured to be zero, can we ascertain that the compact object is a Kerr black hole.

Motivated by examining the no-hair theorem, Johannsen and Psaltis [10] applied recently the Newman-Janis transformation [11] and constructed a Kerr-like black hole metric with a deformed parameter ϵ , which measures potential deviations from the Kerr geometry. This rotating black hole possesses some striking properties. For example, there are no restrictions on the values of the rotation parameter a and the deformation parameter ϵ , which means that it is possible that the rotation parameter is larger than the mass of the black hole in this spacetime. Moreover, the radius of horizon of the rotating non-Kerr black hole depends on the Boyer-Lindquist polar angular coordinate θ , and the spacetime is free of closed timelike curves outside of the outer horizon [10]. Especially, as the deformation parameter $\epsilon > 0$, the black hole possesses two disconnected spherical horizons for a high rotation parameter and has no horizon for $a > M$. When $\epsilon < 0$, the horizon always exists for the arbitrary a , but the topology of the horizon becomes toroidal [12, 13]. The asymptotic behaviors of such a black hole in the weak field approximation are the same as those of the usual Kerr black hole in general relativity [10]. These special properties have attracted recently a great interest in the study of the rotating non-Kerr black hole [10, 12–17].

Gravitational lensing is such a phenomenon resulting from the deflection of light rays in a gravitational field. Like a natural and large telescope, gravitational lensing can help us extract the information about the distant stars which are too dim to be observed. The strong gravitational lensing is caused by a compact object with a photon sphere. When the photons pass close to the photon sphere, the deflection angles become so large that an observer would detect two infinite sets of faint relativistic images on each side of the black hole, which are produced by photons that make complete loops around the black hole before reaching the observer.

These relativistic images can provide us not only some important signatures about black holes in the Universe, but also profound verification of alternative theories of gravity in their strong field regime [18–24]. Thus, the strong gravitational lensing is regarded as a powerful indicator of the physical nature of the central celestial objects and then has been studied extensively in various theories of gravity [18, 25–37].

The main purpose of this paper is to study the strong gravitational lensing by a rotating non-Kerr compact object and to see whether it can leave us the signature of the deformation parameter in the deflection angle, the coefficients, and the observables for gravitational lensing in the strong field limit. Moreover, we will explore how it differs from the Kerr black hole lensing.

The paper is organized as follows: In the following section, we will review briefly the rotating no-Kerr black hole metric proposed by Johannsen and Psaltis [10] to test the no-hair theorem in the strong field regime, and then study the deflection angles for light rays propagating in this background. In Sec.III, we study the physical properties of the strong gravitational lensing by the rotating non-Kerr compact object and probe the effects of the deformation parameter on the marginally circular photon orbit radius, the deflection angle, the coefficients, and the observables for gravitational lensing in the strong field limit. We end the paper with a summary.

II. ROTATING NON-KERR BLACK HOLE SPACETIME AND THE DEFLECTION ANGLES FOR LIGHT RAYS

Let us now first review briefly the rotating no-Kerr black hole metric, which was proposed by Johannsen and Psaltis [10] to test gravity in the strong field regime. Beginning with a deformed Schwarzschild solution and applying the Newman-Janis transformation, they constructed a deformed Kerr-like metric with three parameters: the mass M , the rotation parameter a , and the deformation parameter ϵ . It is a stationary, axisymmetric, and asymptotically flat spacetime. The line elements of the rotating no-Kerr black hole in the standard Boyer-Lindquist coordinates can be expressed as [10]

$$ds^2 = g_{tt}dt^2 + g_{rr}dr^2 + g_{\theta\theta}d\theta^2 + g_{\phi\phi}d\phi^2 + 2g_{t\phi}dtd\phi, \quad (1)$$

where

$$\begin{aligned} g_{tt} &= -\left(1 - \frac{2Mr}{\rho^2}\right)(1+h), & g_{t\phi} &= -\frac{2aMr\sin^2\theta}{\rho^2}(1+h), \\ g_{rr} &= \frac{\rho^2(1+h)}{\Delta + a^2h\sin^2\theta}, & g_{\theta\theta} &= \rho^2, \\ g_{\phi\phi} &= \sin^2\theta\left[r^2 + a^2 + \frac{2a^2Mr\sin^2\theta}{\rho^2}\right] + \frac{a^2(\rho^2 + 2Mr)\sin^4\theta}{\rho^2}h, \end{aligned} \quad (2)$$

with

$$\rho^2 = r^2 + a^2 \cos^2 \theta, \quad \Delta = r^2 - 2Mr + a^2, \quad h = \frac{\epsilon M^3 r}{\rho^4}. \quad (3)$$

The deformed parameter $\epsilon > 0$ or $\epsilon < 0$ corresponds to the cases in which the compact object is more prolate or oblate than a Kerr black hole, respectively. As $\epsilon = 0$, the black hole is reduced to the usual Kerr black hole in general relativity. The position of the black hole horizon is defined by [12, 13]

$$\Delta + a^2 h \sin^2 \theta = 0. \quad (4)$$

It is obvious that the radius of horizon is a function of the Boyer-Lindquist polar angle θ , which is quite a different from that in the usual Kerr case. For the case $\epsilon > 0$, one can find that there exist two disconnected spherical horizons for high spin parameters, but there is no horizon for $a > M$. However, for $\epsilon < 0$, it is shown that the horizon never disappears for the arbitrary a and the shape of the horizon becomes toroidal [12, 13]. Moreover, one can find that it is free of closed timelike curves and then causality is satisfied outside of the event horizon [10].

Let us now study the strong gravitational lensing by a rotating non-Kerr compact object. For simplicity, we here just consider that both the observer and the source lie in the equatorial plane in the rotating non-Kerr black hole spacetime (1) and the whole trajectory of the photon is limited on the same plane. With this condition $\theta = \pi/2$, we obtain the reduced metric in the form

$$ds^2 = -A(x)dt^2 + B(x)dx^2 + C(x)d\phi^2 - 2D(x)dt d\phi, \quad (5)$$

where we adopt to a new radial coordinate $x = r/2M$ and then the metric coefficients become

$$A(x) = \left(1 - \frac{1}{x}\right) \left(1 + \frac{\epsilon}{8x^3}\right), \quad (6)$$

$$B(x) = \frac{x^2(8x^3 + \epsilon)}{8x^4(x-1) + a^2(8x^3 + \epsilon)}, \quad (7)$$

$$C(x) = x^2 + a^2 + \frac{a^2(8x^3 + \epsilon + x\epsilon)}{8x^4}, \quad (8)$$

$$D(x) = \frac{a(8x^3 + \epsilon)}{8x^4}. \quad (9)$$

The null geodesics for the metric (5) has the form

$$\frac{dt}{d\lambda} = \frac{C(x) - JD(x)}{D(x)^2 + A(x)C(x)}, \quad (10)$$

$$\frac{d\phi}{d\lambda} = \frac{D(x) + JA(x)}{D(x)^2 + A(x)C(x)}, \quad (11)$$

$$\left(\frac{dx}{d\lambda}\right)^2 = \frac{C(x) - 2JD(x) - J^2A(x)}{B(x)C(x)[D(x)^2 + A(x)C(x)]}. \quad (12)$$

where λ is an affine parameter along the geodesics and J is the angular momentum of the photon. In the background of a rotating non-Kerr compact object (1), one can obtain the relation between the impact parameter $u(x_0)$ and the distance of the closest approach of the light ray x_0 by the conservation of the angular momentum of the scattering process

$$u(x_0) = J(x_0) = \frac{8x_0^6 + a^2(x_0 + 1)(8x_0^3 + \epsilon)}{a(8x_0^3 + \epsilon) + x_0\sqrt{(8x_0^3 + \epsilon)[8(x_0 - 1)x_0^4 + a^2(8x_0^3 + \epsilon)]}}. \quad (13)$$

Moreover, the deflection angle of the light becomes unboundedly large as the closest distance of approach x_0 tends to the marginally stable orbit radius x_{ps} of the photon. In a stationary, axially-symmetric metric, the equation of circular photon orbits reads

$$A(x)C'(x) - A'(x)C(x) + 2J[A'(x)D(x) - A(x)D'(x)] = 0. \quad (14)$$

The biggest real root external to the horizon of this equation defines the marginally stable circular radius of photon $x_{ps} = r_{ps}/2M$. For a rotating non-Kerr metric (1), the equation of circular photon orbits takes the form

$$128x^9[x(2x - 3)^2 - 8a^2] + 32x^6(10x^3 - 27x^2 + 18x - 18a^2)\epsilon + 2x^3[x(5x - 6)^2 - 48a^2]\epsilon^2 - 5a^2\epsilon^3 = 0. \quad (15)$$

Obviously, this equation depends on both the deformed parameter ϵ and the rotation parameter a of the compact object. The presence of the deformed parameter ϵ makes the equation more complex so that it is impossible to get an analytical form for the marginally circular photon orbit radius in this case. In Fig.(1), we present the variety of the marginally circular photon orbit radius x_{ps} with the deformed parameter ϵ and the rotation parameter a by solving Eq. (15) numerically. It is shown that the marginally circular photon orbit radius x_{ps} decreases with the rotation parameter a and the deformed parameter ϵ . This implies the variety of the marginally circular photon orbit radius x_{ps} with the rotation parameter a which is similar to that in the Kerr black hole spacetime. Moreover, we also find that the marginally circular photon orbit radius x_{ps} always exists for the case where the black hole is more oblate than a Kerr black hole (i.e., $\epsilon < 0$) or the case in which the black hole rotates in the converse direction as the photon (i.e., $a < 0$). When the black hole is prolate ($\epsilon > 0$) and it rotates in the same direction as the photon ($a > 0$), the marginally circular photon orbit exists only in the regime $\epsilon < \epsilon_{max}$ for fixed a . The value of ϵ_{max} is defined by the condition that the marginally circular photon orbit is overlapped with the event horizon (i.e., $x_{ps} = x_H$). In Table (I), we present the largest value of the deformed parameter ϵ_{max} still holding up the marginally circular photon orbit for fixed a , which shows that it decreases with the parameter a . When $\epsilon > \epsilon_{max}$, both the marginally circular photon orbit and

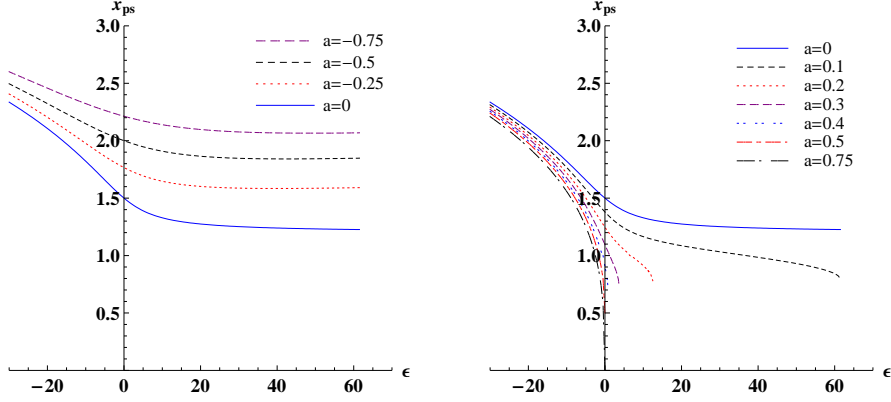


FIG. 1: Variety of the marginally circular orbit radius of the photon with the deformed parameter ϵ for different a . Here, we set $2M = 1$.

a	0	0.1	0.2	0.3	0.4	0.5
ϵ_{max}	∞	61.50	12.52	3.705	0.927	0
$\lim_{\epsilon \rightarrow \epsilon_{max}} x_{ps}$	1.2	0.792	0.770	0.726	0.653	0.5

TABLE I: The upper limit of the deformed parameter ϵ still holding up the marginally circular photon orbit.

the event horizon vanish and then the singularity is naked, which means that in this case the gravitational lensing does not give relativistic images because of the nonexistence of the marginally circular orbit of photon. This information implies that the gravitational lensing by a rotating non-Kerr compact object possesses some new special features, which could provide a possibility to test the no-hair theorem in the strong field regime in the near future.

The deflection angle for the photon coming from infinite in a stationary, axially-symmetric spacetime, described by the metric (5) obeys [38]

$$\alpha(x_0) = I(x_0) - \pi, \quad (16)$$

where $I(x_0)$ is given by

$$I(x_0) = 2 \int_{x_0}^{\infty} \frac{\sqrt{B(x)|A(x_0)|}[D(x) + JA(x)]dx}{\sqrt{D^2(x) + A(x)C(x)}\sqrt{A(x_0)C(x) - A(x)C(x_0) + 2J[A(x)D(x_0) - A(x_0)D(x)]}}. \quad (17)$$

It is obvious that the deflection angle increases when parameter x_0 decreases. For a certain value of x_0 the deflection angle becomes 2π , so that the light ray makes a complete loop around the lens before reaching the observer. If x_0 is equal to the radius of the marginally circular photon orbit x_{ps} , one can find that the deflection angle becomes unboundedly large and the photon is captured on a circular orbit. Let us now discuss

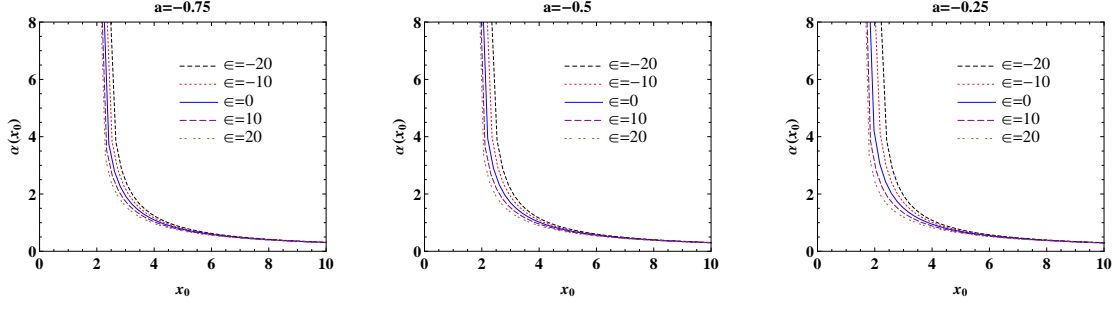


FIG. 2: Deflection angle $\alpha(x_0)$ as a function of the closest distance of approach x_0 for angular momentum $a < 0$. Here, we set $2M = 1$.

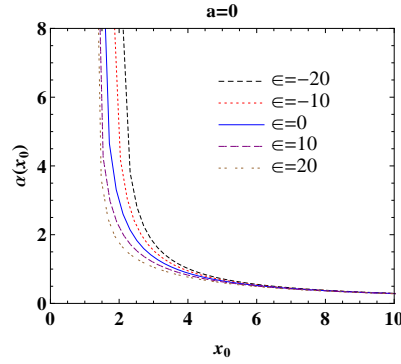


FIG. 3: Deflection angle $\alpha(x_0)$ as a function of the closest distance of approach x_0 for angular momentum $a = 0$. Here, we set $2M = 1$.

the behavior of the deflection angle for the lens described by a rotating non-Kerr metric (1). From Figs. (2)-(4), one can find that $\lim_{x_0 \rightarrow \infty} \alpha(x_0) = 0$ for all values of ϵ and the angular momentum a , which is the same as that in the Kerr case. When there exists a marginally circular photon orbit for the compact object, we find that the deflection angle has similar qualitative behavior for the different deformed parameter ϵ and it strictly increases with the decreases of the impact parameter and becomes unboundedly large as the closest distance of approach x_0 tends to the respective marginally circular orbit radius x_{ps} , i.e., $\lim_{x_0 \rightarrow x_{ps}} \alpha(x_0) = \infty$ for $a < 0$ and $a > 0$, $\epsilon < \epsilon_{max}$. When there does not exist a marginally circular photon orbit and the singularity is naked, we find that the deflection angle of the light ray closing to the singularity tends to a certain positive finite value α_s , i.e., $\lim_{x_0 \rightarrow 0} \alpha(x_0) = \alpha_s$ for $a > 0$, $\epsilon > \epsilon_{max}$. This is not surprising, because in this case the event horizon has disappeared so that the photon could not be captured by the rotating non-Kerr compact object. Moreover, the similar behavior of the deflection angle was also obtained in the Janis-Newman-Winicour spacetime with the naked singularity [22, 26]. The unique difference is that the finite deflection angle is positive in the rotating non-Kerr spacetime (1) and is negative in the Janis-Newman-Winicour spacetime [22, 26], which could be explained by the fact that the difference in the spacetime structures between the rotating non-Kerr spacetime

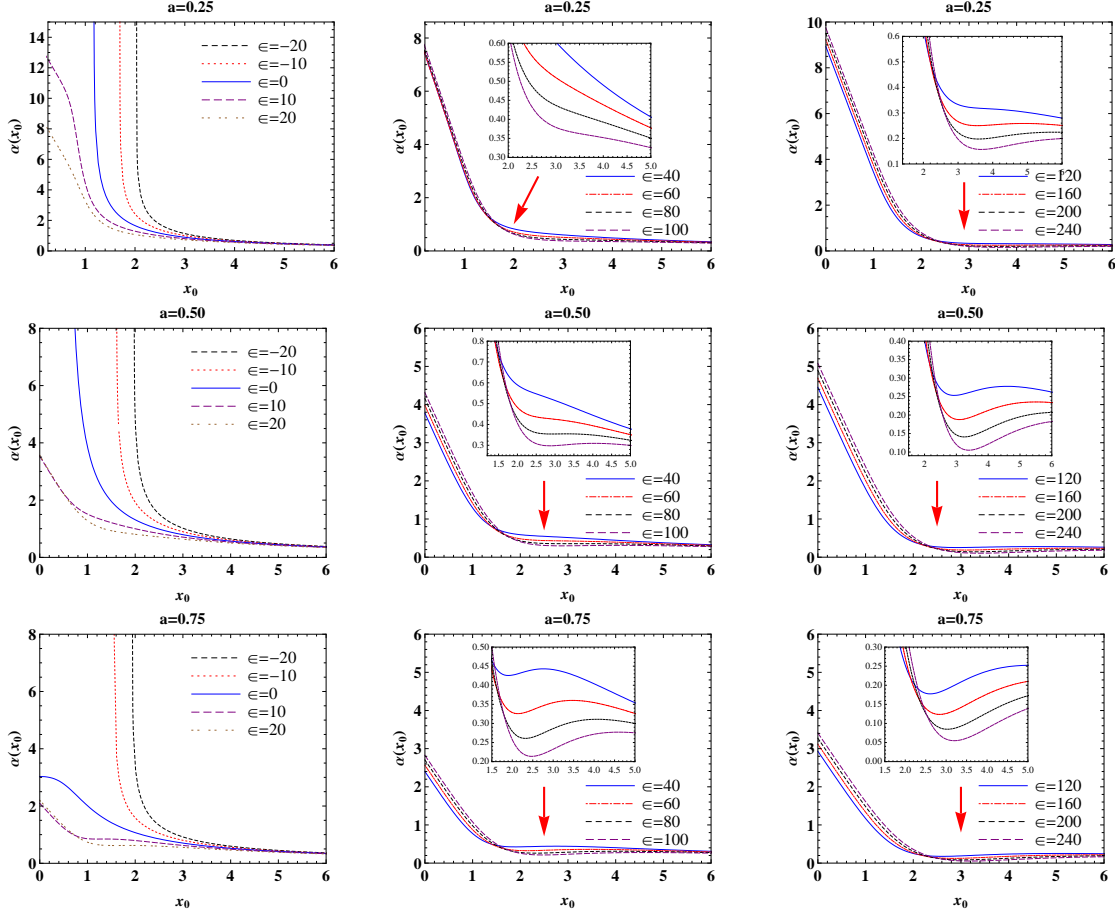


FIG. 4: Deflection angle $\alpha(x_0)$ as a function of the closest distance of approach x_0 for angular momentum $a > 0$. Here, we set $2M = 1$.

and the Janis-Newman-Winicour spacetime leads to the different properties of the naked singularities. This implies that the gravitational lensing could provide a possible way to distinguish the singularities in various spacetimes. The change of α_s with the deformed parameter ϵ and the angular momentum a is shown in Fig. (5), which tells us that it decreases monotonically with a and first decreases and then increases with the deformed parameter ϵ . Moreover, we also note that for the larger deformed parameter ϵ and angular momentum a there exists a minimum for the deflection angle, which depends on the parameters ϵ and a .

III. STRONG GRAVITATIONAL LENSING IN THE ROTATING NON-KERR SPACETIME

In this section we will study the gravitational lensing by the rotating non-Kerr compact object with the marginally circular photon orbit and then probe the effects of the deformed parameter ϵ on the coefficients and the lensing observables in the strong field limit.

In order to find the behavior of the deflection angle very close to the marginally circular photon orbit, we

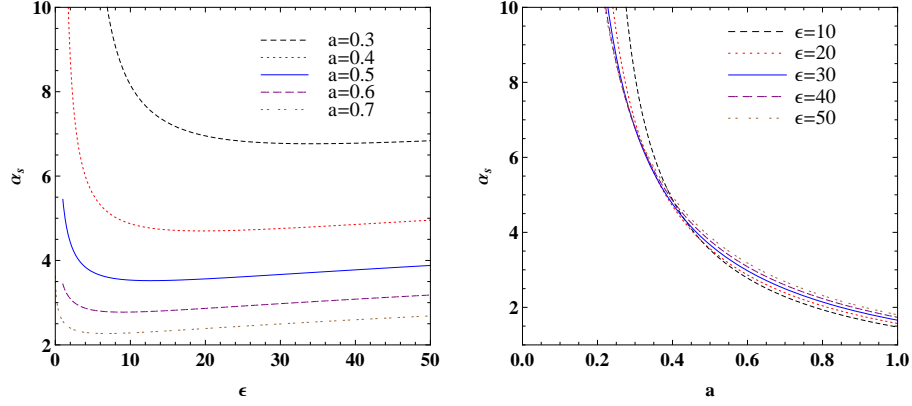


FIG. 5: Variety of the deflection angle α_s with the deformed parameter ϵ and the angular momentum a as the light ray is very close to the singularity. Here, we set $2M = 1$.

adopt the evaluation method for the integral (17) proposed by Bozza [23]. The divergent integral (17) is first split into the divergent part $I_D(x_0)$ and the regular one $I_R(x_0)$, and then both of them are expanded around $x_0 = x_{ps}$ and with sufficient accuracy are approximated with the leading terms. This technique has been widely used in studying the strong gravitational lensing of various black holes [18–36]. Let us now to define a variable

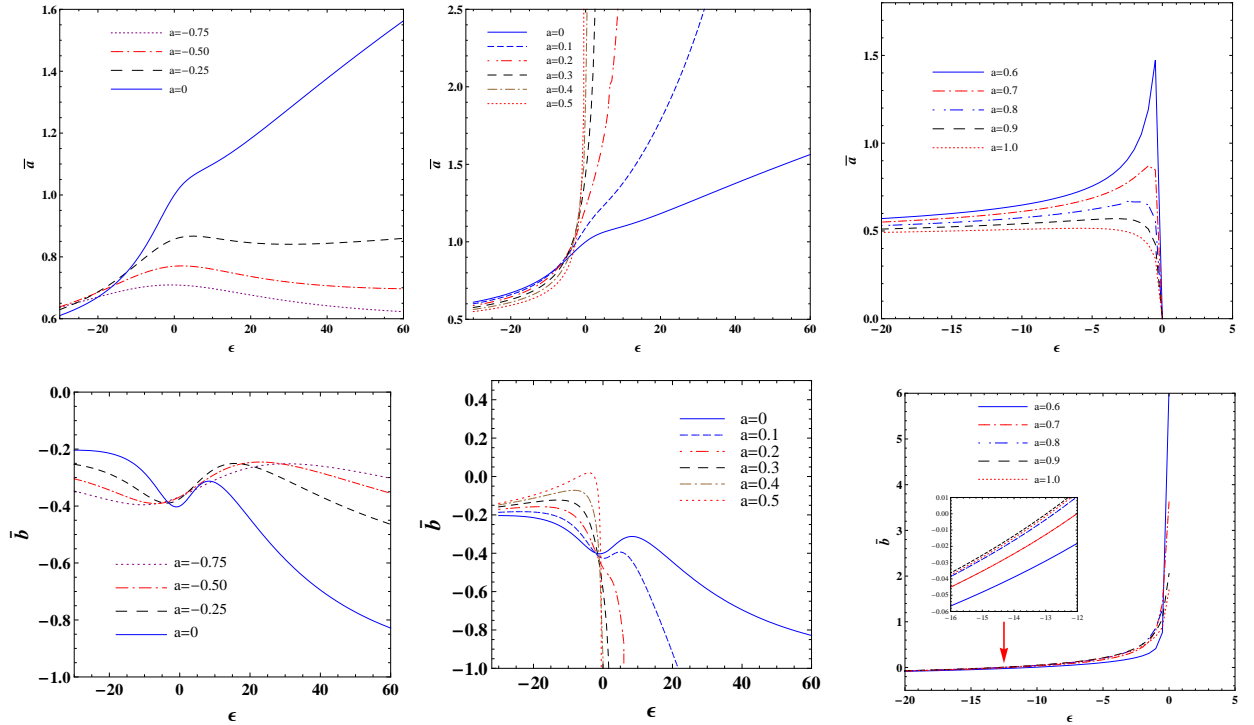


FIG. 6: Change of the strong deflection limit coefficients with the deformed parameter ϵ for different a in the rotating non-Kerr spacetime. Here, we set $2M = 1$.

$$z = 1 - \frac{x_0}{x}, \quad (18)$$

and rewrite Eq.(17) as

$$I(x_0) = \int_0^1 R(z, x_0) f(z, x_0) dz, \quad (19)$$

with

$$R(z, x_0) = \frac{2x^2}{x_0 \sqrt{C(z)}} \frac{\sqrt{B(z)|A(x_0)|[D(z) + JA(z)]}}{\sqrt{D^2(z) + A(z)C(z)}}, \quad (20)$$

$$f(z, x_0) = \frac{1}{\sqrt{A(x_0) - A(z) \frac{C(x_0)}{C(z)} + \frac{2J}{C(z)} [A(z)D(x_0) - A(x_0)D(z)]}}. \quad (21)$$

Obviously, the function $R(z, x_0)$ is regular for all values of z and x_0 . However, the function $f(z, x_0)$ diverges

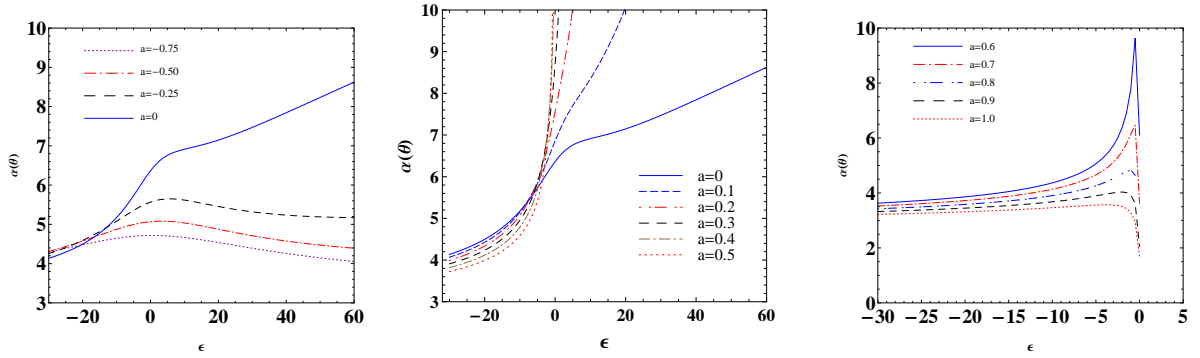


FIG. 7: Deflection angles evaluated at $u = u_{ps} + 0.003$ is a function of the deformed parameter ϵ for different a . Here, we set $2M = 1$.

as z tends to zero, i.e., as the photon approaches the marginally circular photon orbit. Thus, the integral (19) is separated in two parts $I_D(x_0)$ and $I_R(x_0)$

$$\begin{aligned} I_D(x_0) &= \int_0^1 R(0, x_{ps}) f_0(z, x_0) dz, \\ I_R(x_0) &= \int_0^1 [R(z, x_0) f(z, x_0) - R(0, x_{ps}) f_0(z, x_0)] dz. \end{aligned} \quad (22)$$

Expanding the argument of the square root in $f(z, x_0)$ to the second order in z , we have

$$f_0(z, x_0) = \frac{1}{\sqrt{p(x_0)z + q(x_0)z^2}}, \quad (23)$$

where

$$\begin{aligned} p(x_0) &= \frac{x_0}{C(x_0)} \left\{ A(x_0)C'(x_0) - A'(x_0)C(x_0) + 2J[A'(x_0)D(x_0) - A(x_0)D'(x_0)] \right\}, \\ q(x_0) &= \frac{x_0}{2C^2(x_0)} \left\{ 2 \left(C(x_0) - x_0 C'(x_0) \right) \left([A(x_0)C'(x_0) - A'(x_0)C(x_0)] + 2J[A'(x_0)D(x_0) - A(x_0)D'(x_0)] \right) \right. \\ &\quad \left. + x_0 C(x_0) \left([A(x_0)C''(x_0) - A''(x_0)C(x_0)] + 2J[A''(x_0)D(x_0) - A(x_0)D''(x_0)] \right) \right\}. \end{aligned} \quad (24)$$

Comparing Eq.(15) with Eq.(24), one can find that if x_0 approaches the radius of the marginally circular photon orbit x_{ps} the coefficient $p(x_0)$ vanishes and the leading term of the divergence in $f_0(z, x_0)$ is z^{-1} , which implies that the integral (19) diverges logarithmically. The coefficient $q(x_0)$ takes the form

$$q(x_{ps}) = \frac{x_{ps}^2}{2C(x_{ps})} \left\{ A(x_{ps})C''(x_{ps}) - A''(x_{ps})C(x_{ps}) + 2J[A''(x_{ps})D(x_{ps}) - A(x_{ps})D''(x_{ps})] \right\}. \quad (25)$$

Therefore, the deflection angle in the strong field region can be approximated very well as [23]

$$\alpha(\theta) = -\bar{a} \log \left(\frac{\theta D_{OL}}{u_{ps}} - 1 \right) + \bar{b} + \mathcal{O}(u - u_{ps}), \quad (26)$$

with

$$\begin{aligned} \bar{a} &= \frac{R(0, x_{ps})}{\sqrt{q(x_{ps})}}, \\ \bar{b} &= -\pi + b_R + \bar{a} \log \left\{ \frac{2q(x_{ps})C(x_{ps})}{u_{ps}A(x_{ps})[D(x_{ps}) + JA(x_{ps})]} \right\}, \\ b_R &= I_R(x_{ps}), \\ u_{ps} &= \frac{-D(x_{ps}) + \sqrt{A(x_{ps})C(x_{ps}) + D^2(x_{ps})}}{A(x_{ps})}. \end{aligned} \quad (27)$$

The quantity D_{OL} is the distance between the observer and the gravitational lens. Making use of Eqs.(26) and (27), we can study the properties of strong gravitational lensing in the rotating non-Kerr spacetime (1). In Fig.(6), we plotted numerically the changes of the coefficients (\bar{a} and \bar{b}) with the deformed parameter ϵ for different a . It is shown that the coefficients (\bar{a} and \bar{b}) in the strong field limit are functions of the rotation parameter a and the deformed parameter ϵ . For the retrograde photon (i.e., $a < 0$), the coefficient \bar{a} first increases up to its maximum with ϵ , and then decreases down to its minimum with the further increase of ϵ , after that it increases with ϵ . The variety of \bar{b} with ϵ is converse to the variety of \bar{a} with ϵ in this case. When $0 \leq a \leq 0.5$, \bar{a} increases monotonically with ϵ and the behavior of \bar{b} is similar to that in the cases $a < 0$. Both coefficients \bar{a} and \bar{b} diverge as the deformed parameter ϵ tends to the upper limit ϵ_{max} which still holds up a the marginally circular photon orbit. When $a > 0.5$, coefficients \bar{a} and \bar{b} grow with the increase of ϵ . As in the vicinity of the upper limit ϵ_{max} \bar{a} vanishes and \bar{b} tends to a certain positive finite value, which depends on the parameters a and ϵ . The divergence of the coefficients of the expansion implies that the deflection angle in the strong deflection limit (26) is not valid in the regime $\epsilon > \epsilon_{max}$. Moreover, we also note that as the black hole is more oblate, the dependence of the coefficients \bar{a} and \bar{b} on the rotation parameter a is entirely different from those in the usual Kerr black hole. With the increase of a , the coefficient \bar{a} increases as the black hole is prolate (i.e., $\epsilon > 0$) and decreases as the black hole is more oblate. From Fig.(6), one can find

that the variety of \bar{b} with a is converse to the variety of \bar{a} with a . From the above discussion, we know that the change of the coefficients \bar{a} and \bar{b} become more complicated in the rotating non-Kerr spacetime (1). The main reason is that in this spacetime the presence of the deformation parameter ϵ leads to some complicated coupling among the parameters a , ϵ and the polar coordinate x , such as, $a\epsilon$, $a^2\epsilon$, $x^{-3}\epsilon$, $x^2\epsilon$ and $a^2x\epsilon$. The effects of these coupling on the coefficients \bar{a} and \bar{b} are determined not only by the values of the parameters a and ϵ , but also by the signs of a and ϵ . In other words, the dominated coupling terms in the coefficients \bar{a} and \bar{b} are different at different regions of values for the parameters a and ϵ , which yields that \bar{a} and \bar{b} are not the monotonic functions of a and ϵ . The positions of the local minimum and maximum in \bar{a} and \bar{b} are determined by the total effects of these coupling terms and the forms of \bar{a} and \bar{b} themselves. Furthermore, we plotted in Fig. (7) the change of the deflection angles evaluated at $u = u_{ps} + 0.003$ with ϵ for different a as in the regime $\epsilon < \epsilon_{max}$. It is shown that in the strong field limit the deflection angles have similar properties of the coefficient \bar{a} . This means that the deflection angles of the light rays are dominated by the logarithmic term in this case.

Let us now study the effect of the deformed parameter ϵ on the observational gravitational lensing parameters in the strong field limit. When the source and observer are far enough from the lens, the lens equation can be approximated well as [24]

$$\gamma = \frac{D_{OL} + D_{LS}}{D_{LS}}\theta - \alpha(\theta) \mod 2\pi \quad (28)$$

where D_{LS} is the lens-source distance and D_{OL} is the observer-lens distance. γ is the angle between the direction of the source and the optical axis. $\theta = u/D_{OL}$ is the angular separation between the lens and the image. Following Ref.[24], we here consider only the case in which the source, lens and observer are highly aligned. In this limit, one can find that the angular separation between the lens and the n -th relativistic image is

$$\theta_n \simeq \theta_n^0 \left(1 - \frac{u_{ps}e_n(D_{OL} + D_{LS})}{\bar{a}D_{OL}D_{LS}} \right), \quad (29)$$

with

$$\theta_n^0 = \frac{u_{ps}}{D_{OL}}(1 + e_n), \quad e_n = e^{\frac{\bar{b} + |\gamma| - 2\pi n}{\bar{a}}}. \quad (30)$$

The quantity θ_n^0 is the image position corresponding to $\alpha = 2n\pi$, and n is an integer. According to the past oriented light ray which starts from the observer and finishes at the source the resulting images stand on the eastern side of the black hole for direct photons ($a > 0$) and are described by positive γ . Retrograde

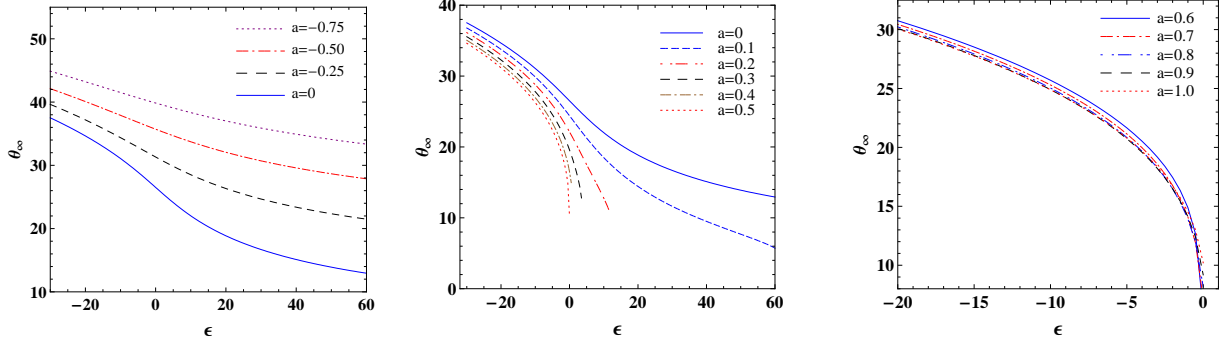


FIG. 8: Variety of the innermost relativistic image θ_∞ with the deformed parameter ϵ for different a . Here, we set $2M = 1$.

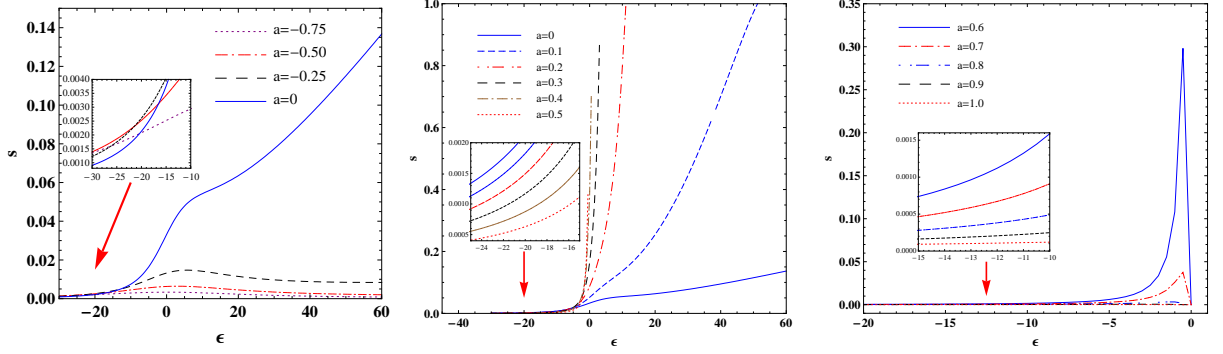


FIG. 9: Variety of the angular separation s with the deformed parameter ϵ for different a . Here, we set $2M = 1$.

photons ($a < 0$) have images on the western side of the black hole and are described by negative values of γ . In the limit $n \rightarrow \infty$, one can find that $e_n \rightarrow 0$, which means that the relation between the minimum impact parameter u_{ps} and the asymptotic position of a set of images θ_∞ can be simplified further as

$$u_{ps} = D_{OL}\theta_\infty. \quad (31)$$

In order to obtain the coefficients \bar{a} and \bar{b} , one needs to separate at least the outermost image from all the others. As in Refs.[23, 24], we consider here the simplest case in which only the outermost image θ_1 is resolved as a single image and all the remaining ones are packed together at θ_∞ . Thus the angular separation s between the first image and the other ones and the ratio of the flux from the first image and those from all other images \mathcal{R} can be expressed as [23, 24, 26]

$$s = \theta_1 - \theta_\infty = \theta_\infty e^{\frac{\bar{b}-2\pi}{\bar{a}}},$$

$$\mathcal{R} = \frac{\mu_1}{\sum_{n=2}^{\infty} \mu_n} = e^{\frac{2\pi}{\bar{a}}}. \quad (32)$$

Through measuring s , θ_∞ and \mathcal{R} , we can obtain the strong deflection limit coefficients \bar{a} and \bar{b} and the minimum impact parameter u_{ps} . Comparing their values with those predicted by theoretical models, we can

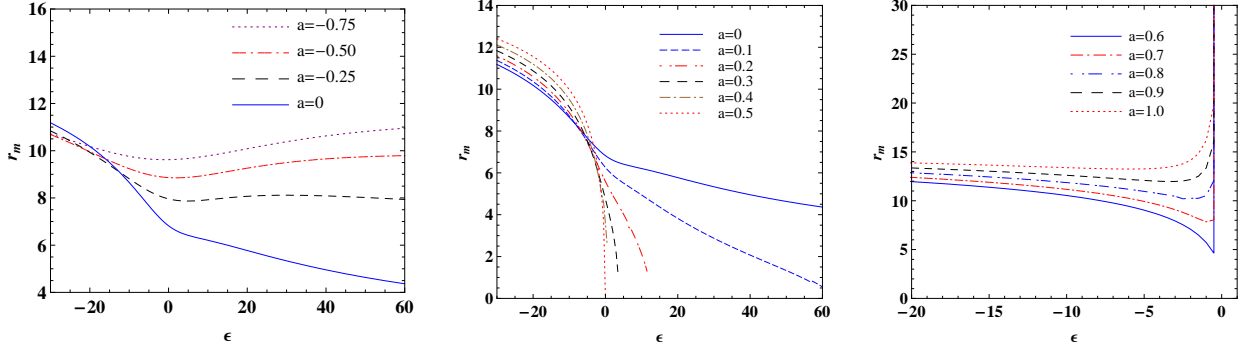


FIG. 10: Variety of the relative magnitudes r_m with the deformed parameter ϵ for different a . Here, we set $2M = 1$.

obtain information about the parameters of the lens object stored in them.

The mass of the central object of our Galaxy was estimated recently to be $4.4 \times 10^6 M_\odot$ [39] and its distance is around $8.5 kpc$, so that the ratio of the mass to the distance $M/D_{OL} \approx 2.4734 \times 10^{-11}$. Making use of Eqs. (27), (31) and (32) we can estimate the values of the coefficients and observables for gravitational lensing in the strong field limit. The numerical value for the angular position of the relativistic images θ_∞ , the angular separation s and the relative magnitudes r_m (which is related to \mathcal{R} by $r_m = 2.5 \log \mathcal{R}$) are plotted in Figs.(8), (9) and (10). In generally, the angular position of the relativistic images θ_∞ decreases with the parameters ϵ and a . While in the vicinity $\epsilon = 0$, it increases with the rotation parameter a as $a > 0.5$. For the retrograde photon (i.e., $a < 0$), the angular separation s between θ_1 and θ_∞ first increases up to its maximum with ϵ , and then decreases down to its minimum with the further increase of ϵ , after that it increases with ϵ . For the prograde photon (i.e., $a > 0$), s increases with ϵ , but near the region $\epsilon \sim 0$ it decreases with ϵ and finally tends to zero as $a > 0.5$. The change of r_m with the parameters ϵ and a is converse to that of the coefficient \bar{a} . Comparing with those in the Kerr background, one find that the behavior of these observable become more complicated since these observable are the functions of the coefficients \bar{a} and \bar{b} , which are related to the parameters a and ϵ with some complex forms. The intrinsic reason is that the presence of ϵ changes the structure of spacetime and makes the motion of the photon more complicated.

IV. SUMMARY

In this paper we have investigated the features of gravitational lensing in a four-dimensional rotating non-Kerr spacetime proposed recently by Johannsen and Psaltis [10] to test the no-hair theorem. Our results show that the deformed parameter ϵ and the rotation parameter a imprint in the marginally circular photon orbit, the deflection angle, the coefficients in strong field lensing and the observational gravitational lensing

variables. We find that the marginally circular photon orbit radius x_{ps} always exists for the cases $\epsilon < 0$ or $a < 0$. But for the case $\epsilon > 0$ and $a > 0$, it exists only in the regime $\epsilon \leq \epsilon_{max}$ for fixed a . The upper limit ϵ_{max} is defined by the critical condition that the marginally circular photon orbit is overlapped with the event horizon. As $\epsilon > \epsilon_{max}$, both the marginally circular photon orbit and the event horizon vanish and then the singularity is naked. The deflection angle of the light ray very close to the naked singularity is a positive finite value, which is different from those in the usual Kerr black hole spacetime and in the rotating naked singularity described by the Janis-Newman-Winicour metric. For all values of a , the relativistic images are closer to the optical axis for a larger deformed parameter ϵ . When $a < 0$, the separability s first increases up to its maximum with ϵ , and then decreases down to its minimum with the further increase of ϵ , after that it increases with ϵ . When $a > 0$, s increases with ϵ , but near the region $\epsilon \sim 0$ it decreases with ϵ and finally tends to zero as $a > 0.5$. The change of r_m with the parameters ϵ and a is converse to that of the coefficient \bar{a} . Moreover, we also note that as the black hole is more oblate, the dependence of the coefficients \bar{a} , \bar{b} and the separability s on the rotation parameter a is entirely different from those in the usual Kerr black hole. These significant features, at least in principle, may provide a possibility to test the no-hair theorem in future astronomical observations.

V. ACKNOWLEDGMENTS

This work was partially supported by the NCET under Grant No.10-0165, the PCSIRT under Grant No. IRT0964 and the construct program of key disciplines in Hunan Province. J. Jing's work was partially supported by the National Natural Science Foundation of China under Grant Nos. 11175065, 10935013; 973 Program Grant No. 2010CB833004.

-
- [1] W. Israel, Phys. Rev. **164** 1776 (1967) ; W. Israel, Commun. Math. Phys. **8** 245 (1968); B. Carter, Phys. Rev. Lett. **26** (1971) 331; S. W. Hawking, Commun. Math. Phys. **25** (1972) 152; D. C. Robinson, Phys. Rev. Lett. **34** 905 (1975).
 - [2] F. D. Ryan, Phys. Rev. D **52** 5707 (1995); L. Barack and C. Cutler, Phys. Rev. D **69** 082005 (2004); J. Brink, Phys. Rev. D **78** 102001 (2008); C. Li and G. Lovelace, Phys. Rev. D **77** 064022 (2008); T. A. Apostolatos, G. Lukes-Gerakopoulos, and G. Contopoulos, Phys. Rev. Lett. **103** 111101 (2009).
 - [3] N. A. Collins and S. A. Hughes, Phys. Rev. D **69** 124022 (2004).
 - [4] S. J. Vigeland and S. A. Hughes, Phys. Rev. D **81** 024030 (2010).
 - [5] J. Gair, C. Li and I. Mandel, Phys. Rev. D **77** 024035 (2008).

- [6] T. Johannsen and D. Psaltis, *Adv. Space Res.* **47** 528 (2011).
- [7] C. Bambi and E. Barausse, *Astrophys. J.* **731** 121 (2011).
- [8] V. S. Manko and I. D. Novikov, *Class. Quantum Grav.* **9** 2477 (1992).
- [9] S. J. Vigeland, N. Yunes, and L. C. Stein, *Phys. Rev. D* **83** 104027 (2011).
- [10] T. Johannsen, D. Psaltis, *Phys. Rev. D* **83** 124015 (2011).
- [11] E. T. Newman and A. I. Janis, *J. Math. Phys.* **6** 915 (1965); S. P. Drake and P. Szekeres, *Gen. Rel. Grav.* **32** 445 (2000).
- [12] C. Bambi, L. Modesto, *Phys. Lett. B* **706** 13 (2011).
- [13] C. Bambi, *Phys. Lett. B* **705** 5 (2011); C. Bambi, L. Modesto, *Phys. Lett. B* **711**, 10 (2012).
- [14] F. Caravelli, L. Modesto, *Class. Quant. Grav.* **27** 245022 (2010).
- [15] P. Pani, C. F. B. Macedo, L. C. B. Crispino, V. Cardoso, *Phys. Rev. D* **84** 087501 (2011).
- [16] T. Johannsen, *Adv. Astron.* **2012**, 486750 (2012), arXiv:1105.5645 [astro-ph.HE].
- [17] S. Chen, J. Jing, *Phys. Lett. B* **711** 81 (2012), arXiv:1110.3462.
- [18] C. Darwin, *Proc. of the Royal Soc. of London* **249** 180 (1959).
- [19] K. S. Virbhadra, D. Narasimha and S. M. Chitre, *Astron. Astrophys.* **337** 1 (1998).
- [20] K. S. Virbhadra, G. F. R. Ellis, *Phys. Rev. D* **62** 084003 (2000).
- [21] C. M. Claudel, K. S. Virbhadra, G. F. R. Ellis, *J. Math. Phys.* **42** 818 (2001).
- [22] K. S. Virbhadra, G. F. R. Ellis, *Phys. Rev. D* **65** 103004 (2002).
- [23] V. Bozza, *Phys. Rev. D* **66** 103001 (2002).
- [24] V. Bozza, *Phys. Rev. D* **67** 103006 (2003);
V. Bozza, F. De Luca, G. Scarpetta, M. Sereno, *Phys. Rev. D* **72** 083003 (2005);
V. Bozza, F. De Luca, G. Scarpetta, *Phys. Rev. D* **74** 063001 (2006).
- [25] G. N. Gyulchev and S. S. Yazadjiev, *Phys. Rev. D* **75** 023006 (2007).
- [26] G. N. Gyulchev and S. S. Yazadjiev, *Phys. Rev. D* **78** 083004 (2008).
- [27] S. Frittelly, T. P. Kling, E. T. Newman, *Phys. Rev. D* **61** 064021 (2000).
- [28] V. Bozza, S. Capozziello, G. Iovane, G. Scarpetta, *Gen. Rel. and Grav.* **33** 1535 (2001).
- [29] E. F. Eiroa, G. E. Romero, D. F. Torres, *Phys. Rev. D* **66** 024010 (2002).
E. F. Eiroa, *Phys. Rev. D* **71** 083010 (2005);
E. F. Eiroa, *Phys. Rev. D* **73** 043002 (2006).
- [30] R. Whisker, *Phys. Rev. D* **71** 064004 (2005).
- [31] A. Bhadra, *Phys. Rev. D* **67** 103009 (2003).
- [32] S. Chen and J. Jing, *Phys. Rev. D* **80** 024036 (2009).
- [33] Y. Liu, S. Chen and J. Jing, *Phys. Rev. D* **81** 124017 (2010); S. Chen, Y. Liu and J. Jing, *Phys. Rev. D* **83** 124019 (2011).
- [34] T. Ghosh, S. Sengupta, *Phys. Rev. D* **81** 044013 (2010).
- [35] A. N. Aliev, P. Talazan, *Phys. Rev. D* **80** 044023 (2009).
- [36] S. Wei, Y. Liu, *Phys. Rev. D* **85**, 064044 (2012).
- [37] G. V. Kraniotis, *Class. Quant. Grav.* **28**, 085021 (2011).
- [38] A. Einstein, *Science* **84** 506 (1936).
- [39] R. Genzel, F. Eisenhauer, S. Gillessen, *Rev. Mod. Phys.* **82**, 3121 (2010), arXiv:1006.0064